Published in final edited form as:
J Neuropathol Exp Neurol. 2013 October ; 72(10): . doi:10.1097/NEN.0b013e3182a5f96e.

Long-term Analyses of Innervation and Neuromuscular Integrity in the Trembler J Mouse Model of Charcot-Marie-Tooth Disease

Jessica R. Nicks, BS, **Sooyeon Lee, PhD**, **Kathryne A. Kostamo, BS**, **Andrew B. Harris**, **Amanda M. Sookdeo, BS**, and **Lucia Notterpek, PhD**
Departments of Neuroscience and Neurology, College of Medicine, McKnight Brain Institute, University of Florida, Gainesville, Florida.

Abstract

A large fraction of hereditary demyelinating neuropathies, classified as Charcot-Marie-Tooth disease type IA (CMT 1A), is associated with misexpression of peripheral myelin protein 22. In this study we characterized morphological and biochemical changes that occur with disease progression in neuromuscular tissue of Trembler J mice, a spontaneous rodent model of CMT 1A. Using age-matched, 2- and 10-month-old wild type and Trembler J mice, we observed neuromuscular deficits that progress from distal to proximal regions. The impairments in motor performance are underlined by degenerative events at distal nerve segments and structural alterations at nerve-muscle synapses. Furthermore, skeletal muscle of affected mice showed reduced myofiber diameter, increased expression of the muscle atrophy marker muscle ring-finger protein 1 and fiber type switching. A dietary intervention of intermittent fasting attenuated these progressive changes and supported distal nerve myelination and neuromuscular junction integrity. In addition to the well-characterized demyelination aspects of this model, our investigations identified distinct degenerative events in distal nerves and muscle of affected neuropathic mice. Therefore, therapeutic studies aimed at slowing or reversing the neuropathic features of these disorders should include the examination of muscle tissue, as well as neuromuscular contact sites.

Keywords

Charcot-Marie-Tooth; Demyelinating neuropathy; Intermittent fasting; Muscle atrophy; Neuromuscular junction; Peripheral myelin protein 22; Peripheral nerve

INTRODUCTION

Hereditary demyelinating peripheral neuropathies afflict approximately 1:2500 in the general population (1) and can have significant impact on the quality of life. Patients with these diseases present with slowed nerve conduction velocity due to myelin abnormalities and axonal degeneration that result in sensory and motor disturbances (2). Changes in neuromuscular physiology include decreased compound muscle amplitudes and smaller motor unit number estimates, both indicative of decreased innervation (3). These abnormalities contribute to the clinical manifestations of the disease including foot drop, muscle weakness and atrophy (4). Deficits in skeletal muscle performance progress with age

Correspondence and reprint requests to: Lucia Notterpek, PhD, Departments of Neuroscience and Neurology, McKnight Brain Institute, 100 Newell Drive, Box 100244, Gainesville, FL 32610-0244. Phone: 352-294-5373; Fax: 352-392-8347; notterpek@ufl.edu.

and are first noticeable in the distal regions of the leg, with advancement into proximal areas (3). In some cases, the disease involves the diaphragm leading to compromised respiratory function (5). Rodents that model these disorders have been well characterized with respect to myelin deficits and Schwann cell abnormalities (6, 7); however, little is known about the involvement of the neuromuscular system in disease progression.

A common form of hereditary neuropathy is Charcot-Marie-Tooth disease type 1A (CMT1A), which is linked to misexpression of peripheral myelin protein 22 (PMP22) (8). While most patients harbor duplication of the PMP22 gene, mutations such as a leucine to proline substitution at amino acid 16 (Leu16Pro) have also been found in human pedigrees and are modeled by the spontaneous mouse mutant Trembler J (TrJ) (9, 10). This mutation is located in the first transmembrane domain of PMP22, and affects the processing and trafficking of the protein (11, 12). In Schwann cells from sciatic nerves of neuropathic mice, PMP22 undergoes altered processing and has a propensity to aggregate (13, 14). Even in normal Schwann cells, PMP22 folds with modest efficiency, with only a small portion of the newly synthesized protein acquiring complex glycosylation and incorporating into myelin (15). In addition, PMP22 harboring the Leu16Pro mutation expressed in TrJ mice has been shown to affect the trafficking of the wild type (Wt) protein, which occurs through dimerization (11). Homozygous TrJ mice die before 3 weeks of age but heterozygous littermates can live past 18 months and exhibit many of the disease phenotypes seen in humans (16, 17). Affected mice show abnormal gait and tremor as early as 1 month of age and the neuropathological findings include reduced axonal diameter, Schwann cell overproliferation, demyelinated axons, and an increase in extracellular collagen deposits (16, 18). It has been hypothesized that these changes in nerve morphology may compromise muscle innervation, as suggested by electromyography (19).

In addition to genetic defects, aging has an impact on peripheral nerve health and function, as well as on nerve-muscle connections. In aged rodents, proximal nerve segments show myelin degeneration, widening of the nodes of Ranvier, and an increase in markers of oxidative damage and immune cell infiltration (20, 21). Muscle innervation becomes compromised over time, with fast-type muscle fibers losing innervation first and then the nerves in slow-type myofibers branching out to compensate for the loss (22). The specialized synapse of peripheral nerves and muscle, the neuromuscular junction (NMJ), shows altered morphology in samples from aged rodents, including axonal thinning and retraction (23). Exercise and calorie reduction are 2 interventions that are known to slow or reverse age-associated degenerative events in multiple tissues, including in the neuromuscular system (20, 23). Specifically, in rodent models of aging, a life-long calorie restriction supports the structural integrity of myelinated nerves and NMJs (23), while an intermittent fasting (IF) (24) regimen slows degenerative events in myelinated nerves of TrJ mice (25).

While the abnormalities in nerve morphology are well documented in PMP22-linked neuropathic models, there are few reports on examining distal regions of neuromuscular tissue. Here we studied TrJ mice over a life-span of 8 months and examined neuromuscular function, distal nerve myelination, muscle innervation, as well as NMJ integrity at 2, 5 and 10 months of age. In an additional cohort of animals, we asked whether the behavioral improvements seen in diet restricted TrJ mice were underlined by improvements in neuromuscular pathology.

MATERIALS AND METHODS

Mouse Colonies and Experimental Design

Age-matched male wild-type (Wt) and heterozygous TrJ mice on the C57Bl/6J background (The Jackson laboratory, Bar Harbor, ME) were offspring from our breeding colony maintained in the McKnight Brain Institute animal facility under specific pathogen-free conditions on a 7:00 AM-7:00 PM light cycle. The University of Florida Institutional Animal Care and Use Committee approved the use of laboratory animals for these studies. For genotyping, DNA was isolated from tail biopsies of 6- to 10-day-old pups and the Leu16Pro mutation was identified by PCR (18). At 9 weeks of age, a cohort of mice was placed on a 5-month-long IF regimen, as described (25).

Behavioral Analyses

Rotarod Test—Age-matched male Wt and TrJ mice were tested at 2, 5, and 10 months on the accelerating Rotarod (Ugo Basile, Camerio VA, Italy) using established procedures (25, 26). Briefly, mice were trained on the Rotarod for 2 consecutive days at constant speed (5 rpm for 60 seconds), and on the third day they were tested on an accelerating Rotarod (4 to 35 rpm over a 300-second-period). The animals completed 3 trials, with a 1-hour rest between trials.

Grip Strength—Forelimb grip strength was measured as tensile force (in pounds) on the Chatillon DFE series Digital Force Gauge apparatus (Chatillon systems, AMETEK Inc., FL) (25). A stainless steel triangle ring was attached to the device. The mouse was gently led to the ring, and front paws were placed in the middle of the triangle ring. Once the grip was established, the mouse was pulled backward until the grip was released. Animals performed 3 trials, with a 5-minute rest between trials.

Rearing Analysis—To measure hind limb strength, mice were tested for rearing behavior, as described (27). Briefly, mice were placed in a glass cylinder, which is a novel environment to facilitate natural rearing behavior. A rearing event is defined as standing on the hind limbs while touching the side of the cylinder with at least 1 front paw. The number of rears was recorded for 10 minutes, with each mouse performing 3 trials with a 20-minute rest between trials.

Primary Antibodies

Chicken anti-phosphorylated neurofilament heavy chain (pNFH), anti-protein 0 (P0) (Western blot) were obtained from Encor Biotechnology, Inc. (Gainesville, FL). Rabbit anti-growth associated protein 43 (GAP43) antibodies were from Abcam (Cambridge, MA). Monoclonal SMI clone 32 antibody from Covance (Princeton, NJ) was used to detect hypo-phosphorylated neurofilament proteins. For the detection of myelin basic protein (MBP), we utilized rat (immunolabeling) and rabbit (Western blot) antibodies, both from Chemicon (Temecula, CA). For muscle tissue analyses, rabbit anti-dystrophin (Abcam) and anti-muscle ring-finger protein 1 (MuRF1) (Santa Cruz Biotechnology, Santa Cruz, CA) antibodies were used. For fiber typing, A4.840 (type I) and SC-71 (type IIa) antibody clones from the Developmental Studies Hybridoma Bank (Iowa City, IA) were utilized.

Immunohistological Analyses

Freshly collected whole soleus muscles (with skin attached for reference) were frozen by immersion in Optimal Cutting Temperature compound cooled with liquid N_2. Samples were sectioned (10- to 20-μm thick) using a Leica CM1850 cryostat and dried onto Superfrost plus slides for 1 hour. Sections were then fixed in 4% paraformaldehyde for 15 minutes,

rinsed in phosphate buffered saline (PBS), and permeabilized using 100% cold methanol. After blocking with 20% goat serum in PBS for 1 hour, sections were incubated with the indicated primary antibodies overnight at 4°C. The following day, the samples were reacted with the appropriate secondary antibodies, and acetylcholine receptors were identified with Alexa-fluor 594-conjugated α-bungarotoxin (α-BTX) (Invitrogen, Grand Island, NY). Nuclei were stained with Hoechst dye (Molecular Probes, Eugene, OR) and coverslips were mounted using a Promega anti-fade kit (Molecular Probes). Tissue sections were imaged using either a Spot camera attached to a Nikon Eclipse E800 microscope, or an Olympus DSU spinning disc confocal camera using Slidebook software and deconvoluted using the standard nearest neighbor algorithm. For semiquantitative assessment, NMJs were identified and analyzed by a blind evaluator, as described (23, 28, 29). Briefly, intact NMJs included α-BTX in close proximity to pNFH-like immunoreactivity, while denervated NMJs were classified as α-BTX labeling without at least 50% of the junction closely adjacent to neurofilament heavy chain (NFH)-like staining. Axonal sprouting was identified by anti-GAP43 antibody-reactive fibers at the nerve terminals. The percent of intact and vacant junctions vs. total junctions in multiple tissue slices were determined for at least 4 mice per age group and genotype. The total number of junctions analyzed per each animal was at least 50.

For quantification of myofiber diameter, 10-μm-thick cross-sections of soleus muscles from Wt and TrJ mice were labeled with an anti-dystrophin antibody. Sections from 4 mice per genotype and age were quantified using Image J. At least 30 fibers were counted per mouse and the average diameter per mouse was calculated. For assessment of fiber types in soleus and extensor digitorum longus (EDL) muscles from Wt and TrJ mice, cross sections were stained with antibodies against myosin heavy chain 2A (Type II) or myosin (Type I). For each muscle section, the number of Type I and Type II fibers was quantified and graphed as percentage of total. At least 3 sections from 3 different mice per age and genotype were assessed.

Biochemical Analyses

Frozen soleus muscles and front and hind paws (3–4 animals from each genotype per age group) were crushed in liquid N_2 and solubilized in tissue lysis buffer supplemented with complete protease inhibitor cocktail (Pierce, Rockford, IL), and phosphatase inhibitor (Sigma, St. Louis, MO). Protein contents of the lysates were determined using the BCA assay kit (Pierce). Muscle (20 μg for muscle and neurofilament proteins, 40 μg for myelin proteins) and paw (40 μg for both neurofilament and myelin proteins) tissue lysates were fractionated by electrophoresis using polyacrylamide gels and then transferred to PVDF membranes. After blocking in 5% nonfat milk in Tris-buffered saline and 0.2% Tween-20, the membranes were incubated with the indicated antibodies overnight at 4°C in 5% BSA. Bound primary antibodies were detected using anti-rabbit, anti-chicken, anti-mouse, or anti-rat horseradish-peroxidase-conjugated secondary antibodies (Cell Signaling, Danvers, MA) and an enhanced chemiluminescent substrate (Perkin Elmer, Boston, MA). Films were digitally imaged using a GS-800 densitometer (Bio-Rad), and bands were quantified using Image J. Semiquantitative analyses of the films were performed after correction for protein loading using glyceraldehyde 3-phosphate dehydrogenase (GAPDH), and normalizing to values of Wt at 2 months of age. Results were verified by repeating the same analyses for each tested antigen on 3 or more independent Western blots on protein samples from different mice. For the IF study, the levels of the studied proteins were normalized to values of Wt, using arbitrary units.

Statistical Analyses

For the accelerating Rotarod behavior study, 2-way ANOVA was used to assess main effects of interactions, and also differences between genotypes at each age. For the other behavior studies and for semiquantitative comparisons, Student t-test from Graphpad prism software (San Diego, CA) was used. When applicable, statistically significant age-effects on the studied parameters are indicated with #.

RESULTS

Trembler J Mice Exhibit Age-Related Declines in Locomotor Performance and Muscle Strength

To assess skeletal muscle function and distal to proximal disease progression, we tested age-matched male Wt and TrJ neuropathic mice at 2, 5 and 10 months of age on 3 different motor behavior tasks (Fig. 1). At the youngest age tested (2 months), TrJ mice were already significantly impaired in their ability to stay on the accelerating Rotarod, with a latency to fall differential of 80 seconds, as compared to Wt (Fig. 1A, ***$p < 0.001$). This finding is in agreement with previous studies using similar aged mice (25, 30, 31). At 5 months of age, TrJ mice continued to show a significant impairment and a decline (#$p < 0.05$) in latency to fall, and performed similarly poorly at the oldest age tested, 10 months. During the same 8-month lifespan, Wt mice maintain performance on the Rotarod without a significant decline. In agreement with the progressive nature of the neuropathy, the differences in performance between the groups become more significant when compared over time (2-way ANOVA, ***$p < 0.001$).

To assess neuropathy-related weakness in specific muscle groups, we analyzed hind limb and forepaw strength using the rearing task (27) and grip strength measures, respectively. Similar to the accelerating Rotarod, there was a genotype effect on rearing task performance throughout the testing, including at 2 months of age (**$p < 0.01$) (Fig. 1B). In addition, neuropathic mice perform significantly worse at 10 months compared to 2 months (#$p < 0.01$), indicating progressive weakness of the hind limbs. In comparison to the Rotarod or rearing tests, we found no significant difference in forepaw grip strength between Wt and neuropathic mice at 2 months of age (Fig. 1C), but at 5 months the forepaw grip strength of neuropathic mice became weaker, and remained impaired at 10 months, vs. age-matched Wt (Fig. 1C). Together, these results show that between the ages of 2 to 10 months, TrJ mice display significant deficits in neuromuscular performance on tests that require muscles of the hind limbs, and only began to show impairment in forelimb strength beginning at 5 months of age.

Distal Nerve Demyelination and Axonal Degeneration in the Soleus Muscle of Neuropathic Mice

Proximal segments of the sciatic nerve from TrJ neuropathic mice show abnormalities as early as 1 month of age (18, 32, 33). To elucidate the distal degenerative events that may underlie the observed neuromuscular deficits, we analyzed the myelin and neuronal protein content of the soleus muscle (which is innervated by branches of the tibial nerve) from 2- and 10-month-old mice. We chose the soleus muscle for assessing distal innervation because it is a well-characterized muscle in normal rodents, as well as in aging and in diseases involving nerve degeneration (29). In whole soleus muscle tissue lysates from neuropathic mice we found a notable decrease in MBP expression at 2 months of age, with nearly complete absence of the protein at 10 months (Fig. 2A). Semiquantitative analyses of independent blots from different samples revealed significant reductions in MBP in neuropathic mice at 2 and 10 months of age vs. Wt, as well as a decline with age (Fig. 2B). P0 levels appeared to be less affected at 2 months, but were significantly reduced in the

older neuropathic mice, a trend that was conformed upon semiquantitative analyses of independent samples (Fig. 2A, B). The pronounced reduction in MBP in 2-month-old TrJ mice is in agreement with the primary dysmyelinating pathology observed in proximal segments of affected sciatic nerves (18).

Next we examined axonal protein content within the same soleus muscle lysates using a panel of antibodies (Fig. 2C). The levels of pNFH were reduced in samples from neuropathic mice at both ages, while SMI32-reactive hypophosphorylated neurofilament levels were elevated (Fig. 2C). Because terminal axon sprouting has been reported in skeletal muscle of neuropathic mice (28), as well as in aged rodents (23), we also studied the expression of GAP43 (34), which in some samples appeared elevated. However, quantitative analyses of independent samples did not confirm this to be significant. In comparison, the observed decrease in pNFH and increase in SMI32-reactive proteins were significant in samples from 10-month-old TrJ mice (** $p < 0.01$, Fig. 2D). In addition, there was an age-associated decrease in pNFH (Fig. 2D, C).

Affected mice show deficits at 2 months of age on the rearing task and the accelerating Rotarod (Fig. 1), both of which require coordinated movement of all muscle groups in the hind paws. To examine myelination and innervation in the hind (H) and forepaws (F), we analyzed whole tissue lysates from Wt and affected mice (Fig. 2E, F). At 2 months of age both front and hind paws of TrJ mice showed pronounced reduction in pNFH, P0 and MBP vs. Wt littermates (Fig. 2E). The reduction in pNFH appeared to be more pronounced in the hind paw as compared to the front paw, while the myelin proteins are severely reduced in both limbs. At 10 months of age, the expression levels of all 3 proteins were further reduced in the neuropathic samples (Fig. 2F). In fact, under the described experimental conditions, the analyzed proteins were barely detectable in the hind paws, indicating a near complete loss of myelinated nerves in distal regions.

To complement the biochemical studies, we examined the soleus muscles of 2- and 10-month-old Wt and TrJ mice by immunohistochemistry using antibodies against myelin and axonal proteins (Fig. 3). In longitudinal sections from young Wt mice, the majority of pNFH-reactive axons were myelinated, as evidenced by ensheathment with MBP-positive Schwann cells (Fig. 3A). Non-myelinated axons were also present in the muscle tissue. In comparison, the samples from a 2-month-old TrJ mouse showed evidence of segmental demyelination (Fig. 3A). In agreement with the pronounced reduction in myelin proteins at 10 months of age (Fig. 2A), we found evidence of segmental demyelination in the muscle tissue from TrJ mice, where many of the pNFH-reactive fibers were devoid of myelin (Fig. 3A, arrowheads). Because biochemical analyses of the soleus muscle revealed some variation in GAP43 between samples from Wt and TrJ mice (Fig. 2C), we stained muscle tissue sections for GAP43 (Fig. 3B). At 2 months of age, GAP43-like staining was observed in close proximity to the post-synaptic acetylcholine receptors in TrJ mice, both within terminal nerve fibers (Fig. 3B, arrowhead) and at the junction (Fig. 3B, arrows). At 10 months of age, GAP43-positive sprouting was still absent in Wt mice at the NMJs, but was present in affected mice (Fig. 3B, arrow). These data indicate that in neuropathic mice, morphological and biochemical changes are occurring along the entire length of the nerve, including segmental demyelination in proximal regions (18) and terminal sprouting at distal sites.

Neuromuscular Junction Abnormalities and Muscle Atrophy in Affected Mice

In normal aging and disease models, the NMJ is susceptible to denervation and morphological alterations (23, 29). To assess the integrity of NMJs within skeletal muscle tissue of TrJ neuropathic mice, whole soleus mounts were stained with anti-pNFH antibody and α-BTX (Fig. 4A-B”). In muscles from 10-month-old Wt mice, the innervation of the

NMJ appeared intact, as indicated by the close apposition of pNFH-reactive nerve terminals with post-synaptic acetylcholine receptor clusters (Fig. 4A). In comparison, skeletal muscle from 10-month-old TrJ mice showed a number of abnormalities, including nerve terminal sprouting (Fig. 4B), axonal thinning (Fig. 4B') and nerve retraction (Fig. 4B"). These pronounced morphological changes at nerve-muscle synapses are in agreement with the behavioral deficits seen in these animals (Fig. 1). To determine if the observed changes are statistically significant, we analyzed muscle tissue sections from multiple age-matched Wt and TrJ mice. Using published methodologies (23, 28), we found that the percentage of intact NMJs, compared to the total number of junctions was significantly lower in affected samples at 10 months vs. age-matched Wt mice (Fig. 4C). Furthermore, there was a highly significant drop-off in the percentage of intact junctions between 5 and 10 months of age, which correlates with poor performance of TrJ mice on the Rotarod and rearing tasks (Fig. 1).

Demyelination and subsequent denervation have been linked to muscle atrophy and changes in muscle composition (35). To examine whether there was skeletal muscle atrophy in our neuropathic mice, we studied several parameters: myofiber diameter, protein markers of atrophy, and myofiber-type composition (Fig. 5). To delineate myofiber diameter, we used an antibody against dystrophin, which connects the cytoskeleton of the muscle fiber to the extracellular matrix (36). On cross-sectional views, fiber diameters in age-matched young Wt and TrJ mice appeared similar but at 10 months there was a notable variation between the genotypes (Fig. 5A). Quantification in samples from 4 mice per age and genotype revealed a significant decrease in myofiber diameter in 10-month-old TrJ mice vs. Wt (Fig. 5B). Moreover, in agreement with the progressive nature of the neuropathy, there was a significant increase in myofiber atrophy between the ages of 2 and 10 months (Fig. 5B; #$p < 0.01$). To examine changes in muscle fiber integrity, we used antibodies against MuRF1, an E3 ubiquitin ligase that is upregulated in skeletal muscles undergoing atrophy (37, 38). As shown on the Western blots, in whole protein lysates of soleus muscles we detected a pronounced increase in MuRF1 protein expression in affected mice, which was significant at 10 months (Fig. 5C, D). Together, these data illustrate myofiber atrophy in response to demyelination-induced denervation in adult TrJ neuropathic mice.

Neuropathic phenotypes are known to elicit heterogeneous changes in skeletal muscle tissue, including a switch from fast type II, to slow type I fibers (35). Typically, nerves innervating fast muscle fibers degenerate first, which leads to a switch in muscle fiber types, as seen in mouse models of amyotrophic lateral sclerosis (29). We examined whether the soleus (composed of type I and II fibers) and EDL (primarily fast-type fibers) undergo fiber type switching in our model by histological examination of fiber type-specific proteins (Fig. 5E, F). In the soleus at 2 months of age, the abundance of type I and II fibers in the soleus were similar in Wt and affected mice; however, at the later time point, type I fibers predominated in both genotypes (Fig. 5E). Quantification of the percentage of type I fibers in independent samples revealed significant age-associated increases in both Wt and TrJ mice (Fig. 5E). In affected mice, over 70% of the myofibers were identified as type I in the soleus at 10 months. In Wt mice, the EDL muscle contained less than 5% slow type fibers at both ages (Fig. 5F), which is in stark contrast to TrJ mice, which had a significant increase in the percentage of slow fibers during the same lifespan. These data reflect changes in the innervation of the soleus and EDL muscles with neuropathy and associated impairment in neuromuscular performance.

An IF Regimen Attenuates Distal Nerve and NMJ Abnormalities

Previously, we have shown that a 5-month-long IF regimen supports locomotor function and proximal sciatic nerve myelination in TrJ neuropathic mice (25). With regards to neuromuscular communication, it is known that lifelong calorie restriction can attenuate

normal aging-related alterations at the NMJ (23). Therefore, we asked whether a 5-month-long IF regimen affects distal nerve myelination and the integrity of NMJs. To determine this, we analyzed whole soleus muscle lysates from TrJ mice fed ad libitum (AL) or IF diet for myelin and axonal proteins using Western blots (Fig. 6A, C). The levels of myelin proteins P0 and MBP appeared higher in samples from the intervention group vs. AL-fed littermates, a trend that was significant upon semiquantitative analyses of independent samples (Fig. 6B). While the improvements in myelin protein expression were significant when compared to AL-fed TrJ mice, the levels did not recover to those in age-matched Wt mice. In comparison, while there was a visible increase in pNFH, these changes are not significant when examined from multiple independent samples. Nevertheless, the levels of SMI32-reactive proteins significantly decrease in mice on the IF regimen (Fig. 6C), and were similar to those in Wt mice. The discrepancy in glial but not axonal improvements may indicate a differential response of Schwann cells and neurons to the IF regimen.

To corroborate the biochemical findings, we performed immunohistochemical analyses on longitudinal sections of soleus muscle from AL and IF-fed TrJ mice (Fig. 6E, F). Immunostaining for myelin and neurofilament proteins revealed prominent MBP-positive myelin sheaths within the tibial nerve of IF-fed neuropathic mice (Fig. 6E, arrows), and fewer demyelinated axonal segments (Fig. 6E, arrowheads). Next, we assessed soleus muscles from the mice for NMJ innervation using anti-pNFH antibodies and α-BTX (Fig. 6F). As shown in the representative images, the alignment of pNFH-positive nerve terminals with α-BTX-reactive post-synaptic sites was improved in samples from the IF group. Indeed, quantification of the percentage of intact NMJs revealed a significant improvement in the intervention group vs. AL-fed TrJ mice (Fig. 6G). Thus, the 5-month-long IF regimen preserved myelin protein expression in distal nerves within the soleus muscles and offered benefits for the innervation of muscle synapses.

DISCUSSION

Our study demonstrates progressive deficits in distal nerve segments in TrJ mice that are associated with impaired neuromuscular performance. Similar to findings in neuropathic patients (39), the abnormalities arise in the longest nerves of the body, in this case those that innervate the hind paws. At 2 months of age, TrJ mice are already debilitated in behavior paradigms requiring hind limb strength and coordination, whereas deficits in forepaw function only became significant around 5 months. These abnormalities in neuromuscular performance are paralleled by loss of myelin proteins in distal nerves, alterations in NMJ innervation and skeletal muscle atrophy. As we previously showed, the IF intervention attenuated many of these functional deficits in TrJ mice (25), and as illustrated here, supported the maintenance of distal myelin and innervation of NMJs. Overall, our findings support the notion that hereditary disease-linked myelin damage affects distal axonal segments and impairs nerve-muscle communication. The mechanisms by which genetic defects within myelinating Schwann cells lead to distal nerve retraction, nerve-muscle synapse dysfunction and skeletal muscle atrophy are not known, but likely to involve multiple pathways.

Studies in rodent models of CMT neuropathies have provided critical insights for understanding the pathogenesis of hereditary demyelinating disorders and offer models for therapy testing (16). However, previous studies of disease pathogenesis have largely focused on Schwann cell demyelination rather than distal axons or neuron-muscle synapses. In one of the early reports on the Trembler mouse, which was later shown to harbor a point mutation in the fourth transmembrane domain of PMP22 (9), Gale et al found terminal sprouting, ultrastructural alterations of the end plates and atrophic muscle fibers (40). The abnormalities in muscle tissue were linked with hypomyelination of the nerves and were

present at 18 days of age, which suggests that these mice were homozygous for the Trembler allele. In a more recent study of a PMP22 overproducing transgenic mouse, in addition to axonal sprouting and NMJ loss, partial muscle denervation was observed (28). The findings in our report agree with these observations and reveal commonalities among 3 distinct mouse models of hereditary demyelination, although with some differences in temporal aspects.

With regards to changes in muscle biology, we extended our study to include muscle fiber typing and analyses of a biochemical marker of muscle atrophy, namely MuRF1. Investigations from rodent models indicate that in response to atrophy or experimental denervation, muscle tissue undergoes adaptive changes that include an increase in MuRF1 protein expression and switch in fiber type (35, 38). It is of note that while at 2 months of age TrJ mice are already severely impaired on the Rotarod and the rearing task, the tested biochemical and morphological markers only revealed fiber type switch in the EDL. It is possible that the early abnormality in neural innervations altered the normal fiber phenotype development of the fast twitch EDL and had less of an impact on the predominantly slow twitch soleus. This hypothesis is supported by studies in mouse embryos, where neural innervation was shown to be critical in determining future muscle phenotype (41). Studies from other neurodegenerative diseases highlight the susceptibility of predominantly fast twitch muscles to denervation-induced fiber type changes (29), which is consistent with our findings in TrJ mice. In addition, early changes in the electrophysiological properties of the muscle and/or the nerve tissue can contribute to functional impairments in the absence of detectable changes in steady-state markers of muscle atrophy. Indeed, a previous publication on 1-month-old TrJ mice detected approximately 20% reduction in motor nerve conduction velocity, which is similar to what has been reported in CMT1A patients with point mutations (17). Furthermore, it is feasible that distal muscles of the hind paws were more affected, which could have impacted performance on the Rotarod. Consistent with this hypothesis, magnetic resonance imaging studies of CMT1A patients with minimal disease phenotype detected selective involvement of intrinsic foot muscles (42).

Electrophysiological properties of neurons are closely linked with the correct expression and localization of axonal proteins and influenced by functional communication with glial cells. Myelination is known to influence the subcellular structure of axons, as in the absence of normal myelination, such as in the Trembler mouse, both quantitative and qualitative properties of slow axonal transport are altered (43). One biochemical marker of axonal degeneration is measurement of the ratios of neurofilament protein isoforms (44, 45). It was recently reported that in the absence of normal myelination there is an increase in the number of nerve fibers that contain nonphosphorylated NFH, as detected with the SMI32 antibody (46). Using this approach, we found a statistically significant increase in SMI32-reactive NFH in soleus samples from 2- and 10-month-old TrJ mice. In comparison, the reduction in phosphorylated NFH within the same lysates was only significant in the older animals. This late decrease in phosphorylated NFH may be a reflection of axon caliber reduction and is in agreement with the progressive nature of the neuropathy, which leads to pronounced axonal degeneration, including a decrease in fiber diameter (18, 33, 47). Subtle biochemical changes in axonal proteins that underlie the behavioral abnormalities in young animals may occur at more distal sites, such as the paws, and contribute to alterations at the NMJ. Alternatively, it is possible that the NMJs in the most distal nerves of TrJ mice are never properly developed, which would agree with the electrophysiological data from the hind feet of 30-day-old animals (19). Finally, it was recently shown that a 10-day-long, short-term demyelination injury can cause significant deficits in locomotor behavior without any change in nerve morphology (48). Therefore, the subcellular alterations that underlie the neuromuscular deficits in TrJ mice likely involve multiple mechanisms within Schwann cells, neurons and myofibers.

In addition to genetic insults, normal aging has a pronounced effect on neuromuscular performance, as well as peripheral nerve morphology and NMJ integrity (49). Studies have shown marked alterations along the entire length of peripheral nerves in aged animals, which include myelin and axonal structures (50). In multiple model systems it is found that neurons with the longest projections are the most prone to age-related abnormalities (51), a result that is recapitulated in TrJ mice. As shown in the results, the neuromuscular tasks that depend on hind limb function deteriorated before those requiring the front paws. This finding agrees with the detection of early abnormalities in the feet of CMT1A patients, which lead to pes cavus with time (42). Therefore, the combined influence of aging and a neuropathic genetic background give rise to abnormalities that surface in the longest nerves of the body.

Interventions that can slow, or reverse age- and genetically-linked degenerative changes within the neuromuscular system are of great interest. In a previous study it was reported that a life-long calorie reduction in mice supports nerve-muscle innervation, including the structure of NMJs (23). Similarly, we have observed the maintenance of myelin and axonal organization, as well as preservation of muscle function in 38-monyh-old rats that were kept on a life-long calorie restricted diet (52, 53). The nerves of diet restricted animals showed a significant decrease in aging-associated abnormalities, including the levels of oxidized and misfolded proteins (21). Moreover, calorie restriction in Drosophila prevented aging-related reduction of synaptic vesicle release from motor neurons (54), indicating that dietary restriction can impact neuronal output. Because neuropathic mice are unable to groom past 1 year of age, our studies with diet restriction utilized a 5-month-long IF regimen, which improved neuromuscular function in both hind and front paws (25). Analyses of the soleus muscle from such mice reveals that these improvements are in part mediated by maintenance of myelin and NMJ integrity. These data demonstrate that the pathological changes in muscles of TrJ mice are amenable to therapy. Dietary restriction acts on multiple protein homeostasis mechanisms, including autophagy and the heat shock pathway (49). It is of interest to identify compounds that mimic the beneficial effects of dietary restriction, as these therapies might be capable of preserving muscle function in healthy aged subjects and/or attenuate deficits in neuropathic patients.

Acknowledgments

The authors wish to thank Dr. Darin Falk and members of the Notterpek lab for helpful discussions, and Doug Smith for technical assistance with the confocal microscopy.

Funding support: NIH-NINDS, National Muscular Dystrophy Association, Trigeminal Neuralgia Association.

REFERENCES

1. Skre H. Genetic and clinical aspects of Charcot-Marie-Tooth's disease. Clin Genet. 1974; 6:98–118. [PubMed: 4430158]
2. Benstead TJ, Grant IA. Progress in clinical neurosciences: Charcot-Marie-Tooth disease and related inherited peripheral neuropathies. Can J Neurol Sci. 2001; 28:199–214. [PubMed: 11513338]
3. Lewis RA, Li J, Fuerst DR, et al. Motor unit number estimate of distal and proximal muscles in Charcot-Marie-Tooth disease. Muscle Nerve. 2003; 28:161–7. [PubMed: 12872319]
4. Murakami T, Garcia CA, Reiter LT, et al. Charcot-Marie-Tooth disease and related inherited neuropathies. Medicine. 1996; 75:233–50. [PubMed: 8862346]
5. Osanai S, Akiba Y, Nakano H, et al. Charcot-Marie-Tooth disease with diaphragmatic weakness. Intern Med. 1992; 31:1267–70. [PubMed: 1295621]
6. Fledrich R, Stassart RM, Sereda MW. Murine therapeutic models for Charcot-Marie-Tooth (CMT) disease. Br Med Bull. 2012; 102:89–113. [PubMed: 22551516]

7. Sereda MW, Nave KA. Animal models of Charcot-Marie-Tooth disease type 1A. Neuromolecular Med. 2006; 8:205–16. [PubMed: 16775377]
8. Li J, Parker B, Martyn C, et al. The PMP22 gene and its related diseases. Mol Neurobiol. 2013; 47:673–98. [PubMed: 23224996]
9. Suter U, Welcher AA, Ozcelik T, et al. Trembler mouse carries a point mutation in a myelin gene. Nature. 1992; 356:241–4. [PubMed: 1552943]
10. Valentijn LJ, Baas F, Wolterman RA, et al. Identical point mutations of PMP-22 in Trembler-J mouse and Charcot-Marie-Tooth disease type 1A. Nat Genet. 1992; 2:288–91. [PubMed: 1303281]
11. Tobler AR, Notterpek L, Naef R, et al. Transport of Trembler-J mutant peripheral myelin protein 22 is blocked in the intermediate compartment and affects the transport of the wild-type protein by direct interaction. J Neurosci. 1999; 19:2027–36. [PubMed: 10066256]
12. Sakakura M, Hadziselimovic A, Wang Z, et al. Structural basis for the Trembler-J phenotype of Charcot-Marie-Tooth disease. Structure. 2011; 19:1160–9. [PubMed: 21827951]
13. Fortun J, Go JC, Li J, et al. Alterations in degradative pathways and protein aggregation in a neuropathy model based on PMP22 overexpression. Neurobiol Dis. 2006; 22:153–64. [PubMed: 16326107]
14. Fortun J, Dunn WA Jr, Joy S, et al. Emerging role for autophagy in the removal of aggresomes in Schwann cells. J Neurosci. 2003; 23:10672–80. [PubMed: 14627652]
15. Pareek S, Notterpek L, Snipes GJ, et al. Neurons promote the translocation of peripheral myelin protein 22 into myelin. J Neurosci. 1997; 17:7754–62. [PubMed: 9315897]
16. Notterpek L, Tolwani RJ. Experimental models of peripheral neuropathies. Lab Anim Sci. 1999; 49:588–99. [PubMed: 10638493]
17. Meekins GD, Emery ML, Weiss MD. Nerve conduction abnormalities in the trembler-j mouse: a model for Charcot-Marie-Tooth disease type 1A? J Peripher Nerv Syst. 2004; 9:177–82. [PubMed: 15363066]
18. Notterpek L, Shooter EM, Snipes GJ. Upregulation of the endosomal-lysosomal pathway in the trembler-J neuropathy. J Neurosci. 1997; 17:4190–200. [PubMed: 9151736]
19. Meekins GD, Carter GT, Emery MJ, et al. Axonal degeneration in the Trembler-j mouse demonstrated by stimulated single-fiber electromyography. Muscle Nerve. 2007; 36:81–6. [PubMed: 17443662]
20. Rangaraju S, Madorsky I, Pileggi JG, et al. Pharmacological induction of the heat shock response improves myelination in a neuropathic model. Neurobiol Dis. 2008; 32:105–15. [PubMed: 18655835]
21. Opalach K, Rangaraju S, Madorsky I, et al. Lifelong calorie restriction alleviates age-related oxidative damage in peripheral nerves. Rejuvenation Res. 2010; 13:65–74. [PubMed: 20230280]
22. Cardasis CA, LaFontaine DM. Aging rat neuromuscular junctions: a morphometric study of cholinesterase-stained whole mounts and ultrastructure. Muscle Nerve. 1987; 10:200–13. [PubMed: 2436045]
23. Valdez G, Tapia JC, Kang H, et al. Attenuation of age-related changes in mouse neuromuscular synapses by caloric restriction and exercise. Proc Natl Acad Sci U S A. 2010; 107:14863–8. [PubMed: 20679195]
24. Klionsky DJ, Abeliovich H, Agostinis P, et al. Guidelines for the use and interpretation of assays for monitoring autophagy in higher eukaryotes. Autophagy. 2008; 4:151–75. [PubMed: 18188003]
25. Madorsky I, Opalach K, Waber A, et al. Intermittent fasting alleviates the neuropathic phenotype in a mouse model of Charcot-Marie-Tooth disease. Neurobiol Dis. 2009; 34:146–54. [PubMed: 19320048]
26. Crawley JN. Behavioral phenotyping of transgenic and knockout mice: experimental design and evaluation of general health, sensory functions, motor abilities, and specific behavioral tests. Brain Res. 1999; 835:18–26. [PubMed: 10448192]
27. Rising AC, Xu J, Carlson A, et al. Longitudinal behavioral, cross-sectional transcriptional and histopathological characterization of a knock-in mouse model of Huntington's disease with 140 CAG repeats. Exp Neurol. 2011; 228:173–82. [PubMed: 21192926]

28. Ang ET, Schäfer R, Baltensperger R, et al. Motor axonal sprouting and neuromuscular junction loss in an animal model of Charcot-Marie-Tooth disease. J Neuropathol Exp Neurol. 2010; 69:281–93. [PubMed: 20142762]
29. Valdez G, Tapia JC, Lichtman JW, et al. Shared resistance to aging and ALS in neuromuscular junctions of specific muscles. PLoS One. 2012; 7:e34640. [PubMed: 22485182]
30. Passage E, Norreel JC, Noack-Fraissignes P, et al. Ascorbic acid treatment corrects the phenotype of a mouse model of Charcot-Marie-Tooth disease. Nat Med. 2004; 10:396–401. [PubMed: 15034573]
31. Khajavi M, Shiga K, Wiszniewski W, et al. Oral curcumin mitigates the clinical and neuropathologic phenotype of the Trembler-J mouse: a potential therapy for inherited neuropathy. Am J Hum Genet. 2007; 81:438–53. [PubMed: 17701891]
32. Robertson AM, Huxley C, King RH, et al. Development of early postnatal peripheral nerve abnormalities in Trembler-J and PMP22 transgenic mice. J Anat. 1999; 195:331–9. [PubMed: 10580849]
33. Henry EW, Sidman RL. The murine mutation trembler-J: proof of semidominant expression by use of the linked vestigial tail marker. J Neurogenet. 1983; 1:39–52. [PubMed: 6681440]
34. Skene JH. Axonal growth-associated proteins. Annu Rev Neurosci. 1989; 12:127–56. [PubMed: 2648946]
35. Maggs AM, Huxley C, Hughes SM. Nerve-dependent changes in skeletal muscle myosin heavy chain after experimental denervation and cross-reinnervation and in a demyelinating mouse model of Charcot-Marie-Tooth disease type 1A. Muscle Nerve. 2008; 38:1572–84. [PubMed: 19016545]
36. Sheard PW, Bewick GS, Woolley AG, et al. Investigation of neuromuscular abnormalities in neurotrophin-3-deficient mice. Eur J Neurosci. 2010; 31:29–41. [PubMed: 20092553]
37. Koyama S, Hata S, Witt CC, et al. Muscle RING-finger protein-1 (MuRF1) as a connector of muscle energy metabolism and protein synthesis. J Mol Biol. 2008; 376:1224–36. [PubMed: 18222470]
38. Bodine SC, Latres E, Baumhueter S, et al. Identification of ubiquitin ligases required for skeletal muscle atrophy. Science. 2001; 294:1704–8. [PubMed: 11679633]
39. Pareyson D, Marchesi C. Diagnosis, natural history, and management of Charcot-Marie-Tooth disease. Lancet Neurol. 2009; 8:654–67. [PubMed: 19539237]
40. Gale AN, Gomez S, Duchen LW. Changes produced by a hypomyelinating neuropathy in muscle and its innervation. Morphological and physiological studies in the Trembler mouse. Brain. 1982; 105:373–93. [PubMed: 6282388]
41. Washabaugh CH, Ontell MP, Shan Z, et al. Role of the nerve in determining fetal skeletal muscle phenotype. Dev Dyn. 1998; 211:177–90. [PubMed: 9489771]
42. Gallardo E, García A, Ramón C, et al. Charcot-Marie-Tooth disease type 2J with MPZ Thr124Met mutation: clinico-electrophysiological and MRI study of a family. J Neurol. 2009; 256:2061–71. [PubMed: 19629567]
43. de Waegh S, Brady ST. Altered slow axonal transport and regeneration in a myelin-deficient mutant mouse: the trembler as an in vivo model for Schwann cell-axon interactions. J Neurosci. 1990; 10:1855–65. [PubMed: 2355253]
44. Cole JS, Messing A, Trojanowski JQ, et al. Modulation of axon diameter and neurofilaments by hypomyelinating Schwann cells in transgenic mice. J Neurosci. 1994; 14:6956–66. [PubMed: 7965091]
45. Perrot R, Berges R, Bocquet A, et al. Review of the multiple aspects of neurofilament functions, and their possible contribution to neurodegeneration. Mol Neurobiol. 2008; 38:27–65. [PubMed: 18649148]
46. Pereira JA, Baumann R, Norrmén C, et al. Dicer in Schwann cells is required for myelination and axonal integrity. J Neurosci. 2010; 30:6763–75. [PubMed: 20463238]
47. Misko A, Ferguson T, Notterpek L. Matrix metalloproteinase mediated degradation of basement membrane proteins in Trembler J neuropathy nerves. J Neurochem. 2002; 83:885–94. [PubMed: 12421361]

48. Napoli I, Noon LA, Ribeiro S, et al. A central role for the ERK-signaling pathway in controlling Schwann cell plasticity and peripheral nerve regeneration in vivo. Neuron. 2012; 73:729–42. [PubMed: 22365547]

49. Lee S, Notterpek L. Dietary restriction supports peripheral nerve health by enhancing endogenous protein quality control mechanisms. Exp Gerontol. Dec 23.2012 doi:pii: S0531-5565(12)00321-X. 10.1016/j.exger.2012.12.008. (Epub ahead of print).

50. Grover-Johnson N, Spencer PS. Peripheral nerve abnormalities in aging rats. J Neuropathol Exp Neurol. 1981; 40:155–65. [PubMed: 7463100]

51. Mattson MP, Magnus T. Ageing and neuronal vulnerability. Nat Rev Neurosci. 2006:7278–94.

52. Rangaraju S, Hankins D, Madorsky I, et al. Molecular architecture of myelinated peripheral nerves is supported by calorie restriction with aging. Aging Cell. 2009; 8:178–91. [PubMed: 19239416]

53. Xu J, Knutson MD, Carter CS, et al. Iron accumulation with age, oxidative stress and functional decline. PLoS One. 2008; 3:e2865. [PubMed: 18682742]

54. Rawson JM, Kreko T, Davison H, et al. Effects of diet on synaptic vesicle release in dynactin complex mutants: a mechanism for improved vitality during motor disease. Aging Cell. 2012; 11:418–27. [PubMed: 22268717]

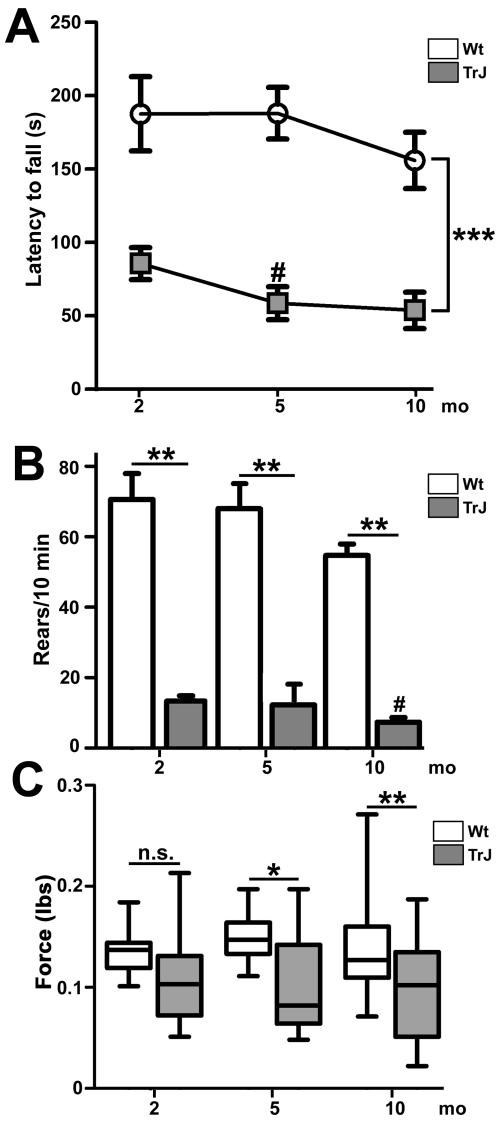

Figure 1.

Age-related declines in neuromuscular performance and muscle strength in Trembler J (TrJ) mice. (**A**) Longitudinal study of performance on the accelerating Rotarod reveals a main effect of genotype (***$p < 0.001$ ANOVA, error bars represent SEM) and a significant decline from baseline at 5 months in TrJ mice (#$p < 0.05$). (**B**) TrJ mice show impairment in rearing behavior at all 3 ages analyzed (**$p < 0.01$, Student t-test, error bars represent SEM), and a decrease in the number of rears between 2 and 10 months (# $p < 0.05$). (**C**) At 2 months of age there is no significant difference in forepaw grip strength between the genotypes, while at 5 and 10 months, forepaw grip strength is reduced in TrJ mice (*$p < 0.05$, Student t test). There is no significant change in forelimb grip strength with age in either genotype. n = 5 to 6 mice/genotype/age group.

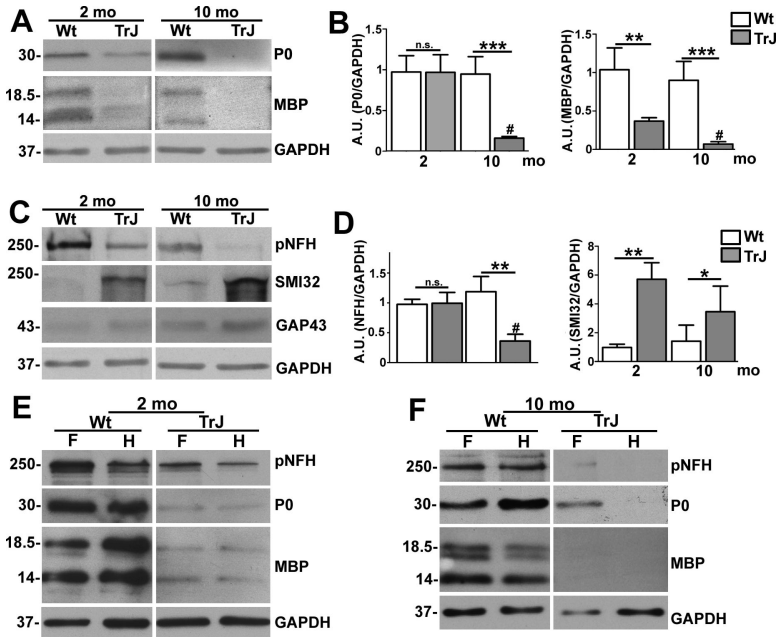

Figure 2.

Progressive demyelination of distal nerve segments. (**A, C**) Whole protein lysates of the soleus muscle (40 μg/lane) from age-matched wild type (Wt) and Trembler J (TrJ) mice were analyzed for myelin (protein zero (P0], myelin basic protein ((MBP]) (**A**) and axonal proteins (phosphorylated neurofilament heavy chain (pNFH), hypo-phosphorylated (NFH] (antibody SMI32], growth associated protein 43 [GAP43]) (**C**). (**B, D**) Semiquantitative analyses of independent blots reveal a significant decrease in P0 and pNFH at 10 months, whereas MBP is reduced and levels of SMI32-reactive NFH are increased at both ages (Student t-test, *$p < 0.05$, **$p < 0.01$, ***$p < 0.001$). In addition, P0, MBP, and pNFH are all significantly decreased in TrJ mice at 10 vs. 3 months (Student t-test, #$p < 0.01$). (**E, F**) Whole protein lysates of front (**F**) and hind (**H**) feet (40 μg/lane) were assessed for neurofilament (pNFH) and myelin protein (P0, MBP) expression from 2-month-old (**E**) and 10 month-old (**F**) Wt and TrJ mice. Glyceraldehyde 3-phosphate dehydrogenase (GAPDH) is the protein loading control (**A, C, E, F**). Molecular mass, in kDa.

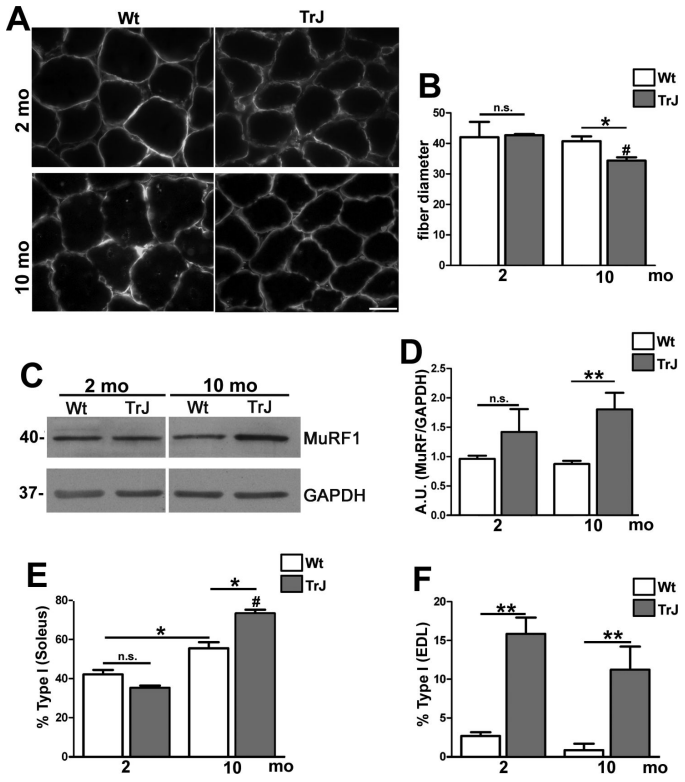

Figure 3.

Decreased myelin-like staining and increased axonal sprouting in soleus muscles of affected mice. (**A**) Longitudinal sections of soleus muscles from 2- and 10-month-old wild type (Wt) and Trembler J (TrJ) mice were co-immunolabeled with anti-myelin basic protein (MBP) (green) and anti-phosphorylated neurofilament-heavy chain (pNFH, red) antibodies. Nuclei are stained blue with Hoechst. MBP-positive myelin sheaths are indicated with filled arrows; demyelinated axons are denoted with arrowheads. Asterisks indicate unmyelinated axons. (**B**) Sections of the soleus muscle from 2- and 10-month-old age-matched Wt and TrJ mice were triple labeled with anti-growth associated protein 43 (GAP43, green), anti-pNFH (blue) antibodies and anti-α-bungarotoxin (α-BTX) (red) to identify acetylcholine receptors. In tissue from 2- and 10-month-old TrJ mice, sprouting was observed throughout in axon fiber tracts (arrowheads), including at the neuromuscular junction (NMJ) (arrows). Axonal sprouting was not seen in Wt mice at either age. Scale bars: **A, B**, 10 μm.

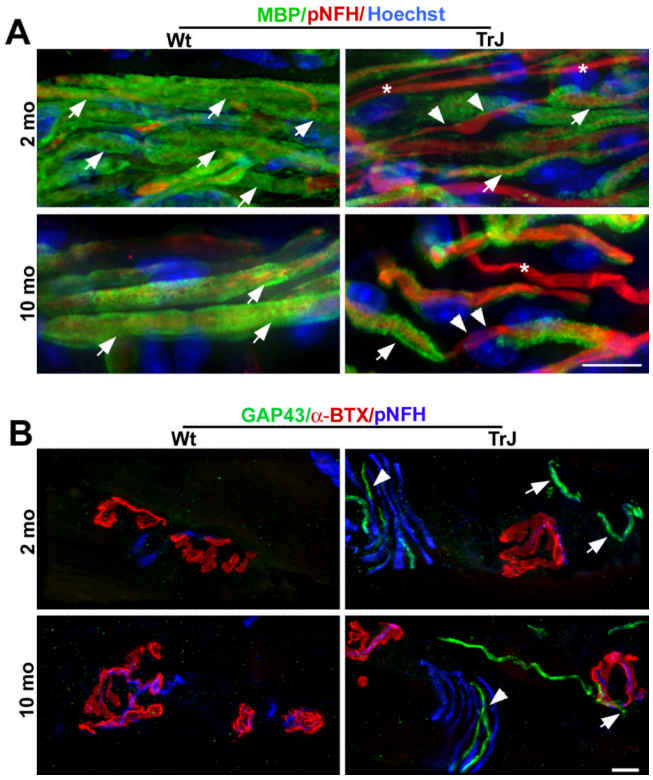

Figure 4.

Compromised neuromuscular junction (NMJ) integrity in the soleus muscle of Trembler J (TrJ) mice. (**A, B**) Longitudinal sections (20 μm thick) from wild type (Wt) (**A**) and TrJ (**B-B”)** soleus muscles were reacted with anti-phosphorylated neurofilament-heavy chain (pNFH) antibody (green) and α-bungarotoxin (α-BTX, red) to stain post-synaptic acetylcholine receptors. Samples from Wt mice (**A**) have thick, well-defined, branched axon terminals in close association with the post-synaptic muscle cell. NMJs from TrJ mice (**B-B”**) show features of altered innervation, i.e. terminal sprouting (**B**, *), thinning (**B’**, arrows) and axon retraction (**B’’**, arrowheads). Scale bar: 10 μm. (**C**) Percentages of intact NMJs were quantified in sections of soleus muscles from Wt and TrJ mice at the indicated ages. At 10 months of age, TrJ mice have a significant reduction compared to both 2 and 5 months (Student t-test, **p < 0.01, ***p < 0.001, #p < 0.01). n = 5 mice per age and genotype.

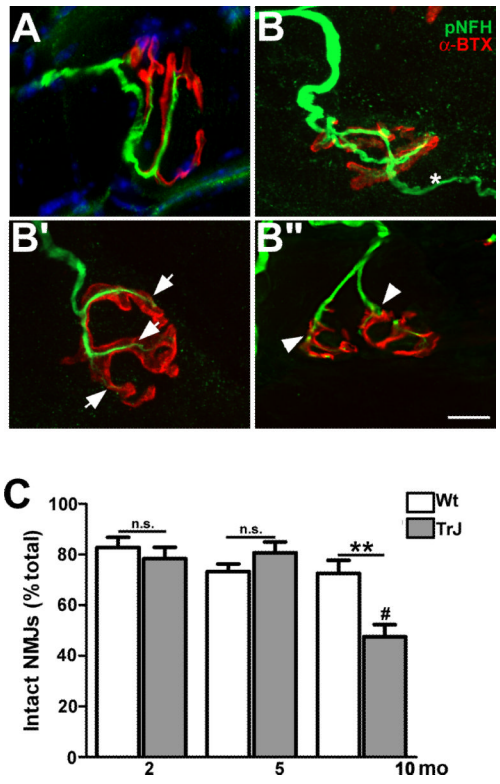

Figure 5.

Skeletal muscle atrophy in aged neuropathic mice. (**A**) Cross sections of soleus muscle from 2- and 10-month-old wild type (Wt) and Trembler J (TrJ) mice were immunolabeled with an anti-dystrophin antibody. Scale bar: 10 μM. (**B**) Quantification of myofiber diameter shows a significant decrease at 10 months in sections from TrJ mice, vs. Wt (Student t-test, *$p < 0.05$). There was no effect of age on fiber diameter in Wt mice, whereas in TrJ mice there was a significant decrease in fiber diameter at 10 months vs. 2 months (Student t-test, # $p < 0.01$). (**C**) Whole soleus muscle lysates (20 μg/lane) were probed for muscle ring-finger protein 1 (MuRF1); glyceraldehyde 3-phosphate dehydrogenase (GAPDH) was the protein loading control. Molecular mass, in kDa. (**D**) Semiquantitative analysis of MuRF1 expression (Student t-test, **$p < 0.01$). (**E, F**) The percentage of Type I (A4.840, red) and Type II (Sc-71, green) myofibers within the soleus (**E**) and extensor digitorum longus (EDL) (**F**) muscles were quantified. In the soleus (**E**), the percentage of Type I fibers shows a significant increase with age in both Wt and TrJ, which is highly significant in the neuropathic condition. In addition, at 10 months there is a significant increase in the percentage of slow-type fibers in TrJ mice vs. Wt (Student t-test, *$p < 0.05$; #$p < 0.01$). The percentage of Type I fibers in the EDL of TrJ mice is higher at 2 and 10 months of age vs. age-matched Wt (Student t-test, **$p < 0.01$) (**F**).

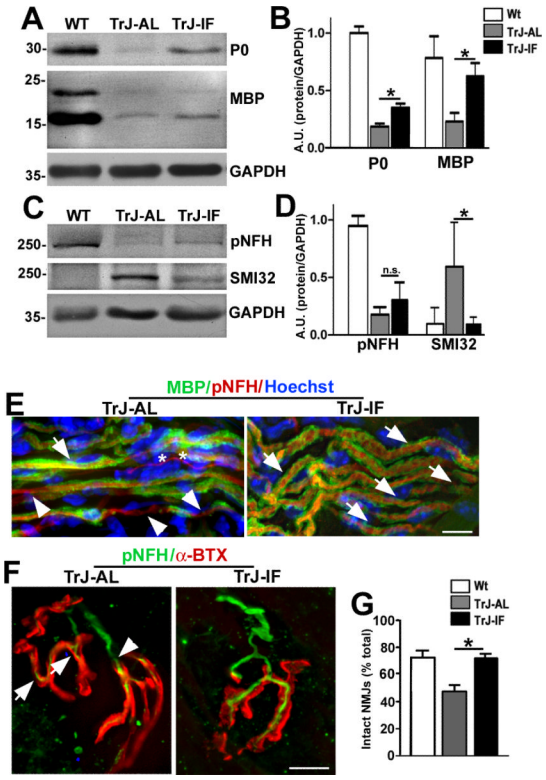

Figure 6.

Intermittent fasting (IF) improves distal nerve myelination and neuromuscular junction (NMJ) innervation. (**A, C**) Whole soleus muscle lysates (40 μg/lane) were analyzed with anti-myelin (myelin basic protein (MBP] and protein zero (P0]), and anti-neurofilament (pNFH and hypo-phosphorylated NFH (SMI32]) antibodies. Glyceraldehyde 3-phosphate dehydrogenase (GAPDH) is shown as a loading control. (**B, D**) Semiquantitative analyses of 4 independent blots. There is a significant increase in the levels of MBP and P0 in samples from intermittent fasted Trembler J (TrJ-IF), vs. ad libitum (AL)-fed littermates (TrJ-AL) (Student t-test, *$p < 0.05$) (**B**). The increased expression of pNFH in TrJ mice on the IF regimen (TrJ-IF) vs. TrJ-AL is not significant but the levels of SMI32-reactive proteins is significantly reduced in IF-fed mice (**D**). (**E**) Sections of soleus muscles from TrJ-AL and TrJ-IF mice were co-immunolabeled with anti-MBP (green) and anti-pNFH (red) antibodies. MBP-positive myelin sheaths (arrows) and demyelinated axon segments (arrowheads) are denoted. Unmyelinated fibers are marked with asterisks. Nuclei are stained with Hoechst dye (blue). (**F**) Sections of soleus muscles from TrJ-AL and TrJ-IF mice were co-labeled with an anti-NFH antibody (green) and α-BTX (red). Thinning (arrows) and axonal retraction (arrowheads) at the NMJs are marked in the NMJ from the TrJ-IF soleus. Scale bars: 10 μm (**E, F**). (**G**) Quantification of intact NMJs in soleus samples from the indicated groups. (Student t-test, *$p < 0.05$). n = 3 to 4 mice per genotype and diet regimen.